

MONITORING OF DAMAGE EVOLUTION AND CRACK LOCALIZATION IN CONCRETE UNDER SPLITTING TEST USING ACOUSTIC EMISSION AND DIGITAL IMAGE CORRELATION

Shahzad Ashraf*,1, Magdalena Rucka1

Abstract

This study focuses on crack monitoring and localisation in concrete cubes reinforced with polymer fibres and steel fibres under a splitting test. Internal cracking behaviour was monitored using the acoustic emission (AE) method, while surface crack localization was achieved with digital image correlation (DIC). The integrated AE and DIC analysis showed that steel fibres can bridge microcracks more effectively than polymer fibres, thereby improving the post-cracking behaviour.

Keywords

Fracture monitoring, Fibre-reinforced concrete, Wedge splitting loading test, Acoustic emission (AE), Digital image correlation (DIC)

1 INTRODUCTION

Concrete remains the predominant used building material component due to its exceptional advantages, including strength, durability, adaptability, and cost-effectiveness. However, its quasi-brittle nature makes it vulnerable to cracking and undergoes significant deformation when subjected to mechanical and environmental stresses. Once microcracks form within the concrete matrix, they gradually accumulate and expand into macrocracks, which can lead to structural failure. Therefore, early identification of crack propagation and continuous real-time monitoring of these cracks is essential to ensure the safety and durability of concrete structures.

Recent advancements in non-destructive testing (NDT) methods have provided highly accurate and reliable methods for early crack detection and damage assessment in materials and structures. Acoustic emission (AE) [1], [2] is the most widely used NDT diagnostic technique, and is valued for its ability to monitor the real-time internal damage and structural integrity in composites. This passive technique detects high-frequency elastic waves generated by the rapid release of strain energy from microstructural changes within materials, which are captured by surface-mounted piezoelectric sensors and converted into electrical signals for detailed analysis. Digital image correlation (DIC) [3], [4] is an advanced non-contact optical technique that uses digital images to make highly accurate quantitative measurements of surface deformation and strain changes within materials. Recent studies have highlighted the benefits of integrating AE and DIC methods, offering a comprehensive approach in which AE focuses on identifying internal damage and DIC focuses on the surface deformation pattern in fibre-reinforced concrete (FRC) [5], [6]. Combining these two techniques, this approach allows for a complete understanding of the fracture behaviour in concrete and helps in identifying critical damage zones before visible signs of macroscopic failure occur. Many researchers are continuously making significant efforts to advance data processing techniques, focusing on the possibility of improving structural damage detection and localization with high accuracy. These efforts play a crucial role in improving the structural assessment process, enabling the early detection of potential failures and facilitating timely maintenance interventions. Ultimately, these advancements contribute to prolonging the service life of concrete infrastructures ensuring their long-term safety and performance.

^{*}shahzad.ashraf@pg.edu.pl

¹ Department of Mechanics of Materials and Structures, Faculty of Civil and Environmental Engineering, Gdańsk University of Technology, Narutowicza 11/12, 80-233, Gdańsk, Poland



The current study focuses on the integrated applications of AE and DIC methods to investigate the real-time monitoring of crack assessment and localization during wedge-splitting tests on concrete cubes. The research involves experimental investigations and in-depth analyses of the damage evolution process in cubic specimens reinforced with polyolefin and steel fibres, utilizing both AE and DIC methods. By adopting this combined approach, the research aims to advance the understanding of real-time fracture dynamics of fibre-reinforced concrete under wedge splitting test and improve the surface crack localization accuracy.

2 METHODOLOGY

Specimens

This study includes experimental tests on three concrete cubic prismatic specimens with dimensions of $7 \times 7 \times 7$ cm³ as depicted in Fig. 1. In order to induce splitting failure, a 4 mm-wide and 15 mm-deep notch was precisely cut at the centre of each specimen. The concrete mix was composed of CEM I 42.5R (330 kg/m³), water (165 kg/m³), fine aggregate (0–2 mm) (710 kg/m³), medium aggregate (2–8 mm) (664 kg/m³), coarse aggregate (8–16 mm) (500 kg/m³). Additionally, a super-plasticizer was incorporated at 0.7% of the cement content to ensure a homogeneous mixture and enhance workability. Three different cubes were prepared: plain concrete (PC) without fibres, polyolefin fibre reinforced concrete (PFRC) containing 0.6% by volume of 24 mm long twisted polyolefin fibres, and steel fibre reinforced concrete (SFRC) with 0.6% by volume of 25 mm long hooked-end steel fibres. The mechanical properties of both polymer and steel fibres are detailed in Tab.1.

Tab. 1 Properties of steel and polyolefin fibres.

Type of fibres	Length (mm)	Diameter (mm)	Tensile strength (MPa)	Elastic modulus (GPa)
polyolefin	24	0.45	600	5
steel	25	0.5	2200	200

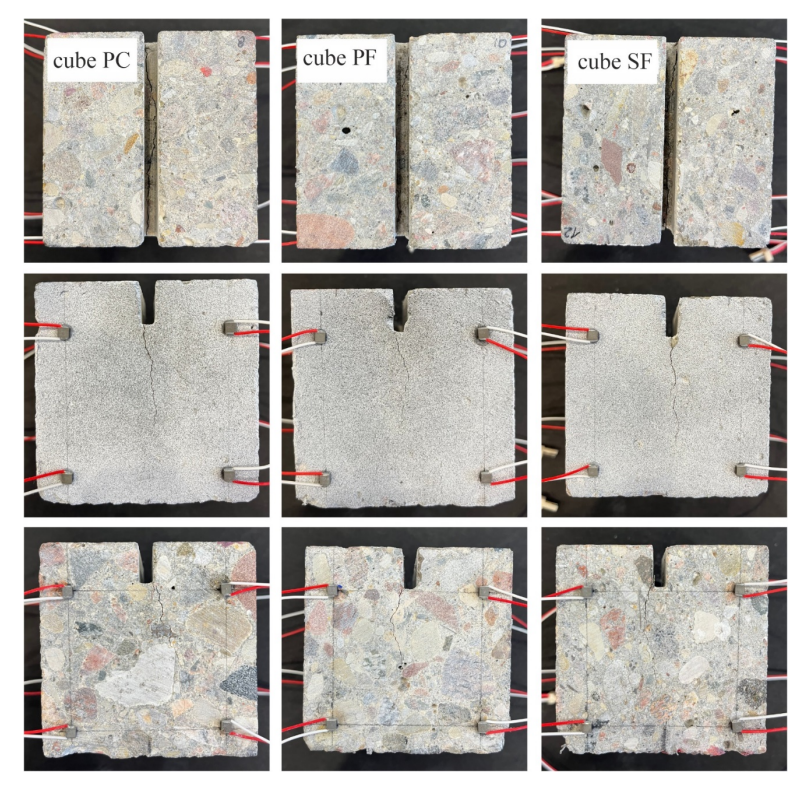


Fig. 1 The views of the concrete cubes after failure with the location of PZT transducers.



Experimental setup

The wedge splitting test (WST) was performed on three concrete cubic specimens labelled as cube PC, cube PF, and cube SF, using a Zwick/Roell Z10 universal testing machine (UTM). To initiate the test, a preload of 20 N was applied, followed by a controlled splitting process at a constant displacement rate of 0.1 mm/min. The tests were stopped after reaching a maximum displacement of 2 mm, which corresponded to 1200 s. To analyze the damage evolution process, a combination of AE and DIC methods were employed simultaneously during quasistatic splitting tests. The AE signals were captured using eight multilayer piezoelectric transducers (NAC2024) produced by Noliac, ensuring precise measurement of crack development and structural response. Of the eight sensors, four were mounted on the front surface of the cubes and four on the rear surface of the cubes, as shown in Fig.2. High-frequency AE signals were recorded with a Vallen AE system, with a threshold value set at 34 dB and a sampling rate of 10 MHz. The crack evolution on the front surface of the cubes was meticulously tracked by capturing high-resolution images every 2 seconds using the ARAMIS MC 3D 12 M system.

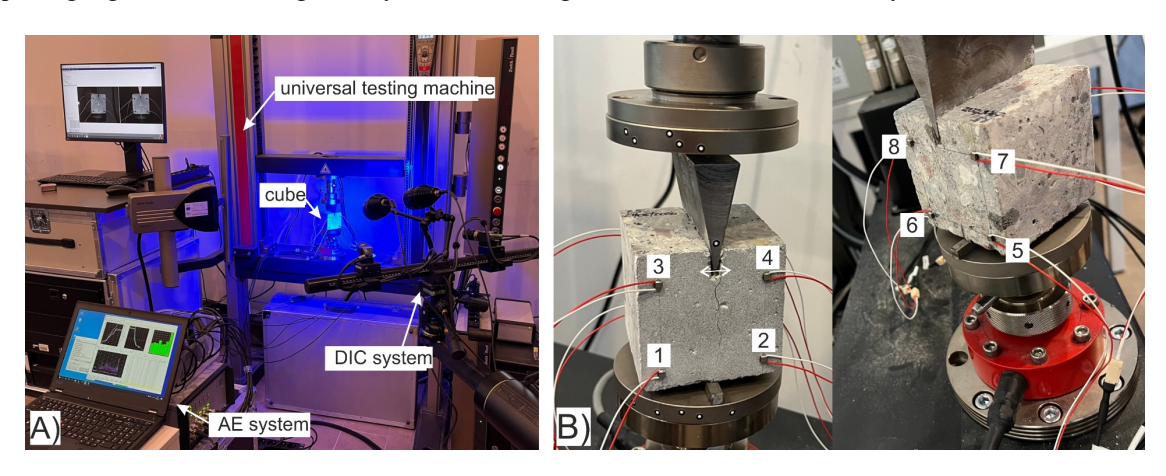


Fig. 2 Experimental setup: A) view of the experimental setup, B) a close-up photograph of the cubic specimen, highlighting the position of AE sensors (numbered 1–8).

3 RESULTS

Quasi-static split test results

Fig. 3(a) illustrates the results of PC, PF and SF prismatic cubic specimens from the quasi-static splitting test. The results of loading vs time were obtained directly from the measuring devices. The peak load values measured for each specimen were as follows: 6014.35 N for plain concrete (PC), 6762.18 N for concrete reinforced with 0.6% polyolefin fibres (PF), and 6449.06 N for concrete with 0.6% steel fibres (SF). Fig. 3(b) displays the load-CMOD curves of tested cubic specimens, which were obtained based on DIC measurements. The load-CMOD curve indicates that during the pre-peak phase, all tested specimens exhibited similar stiffness, whereas the post-peak regime exhibited softening behaviour.



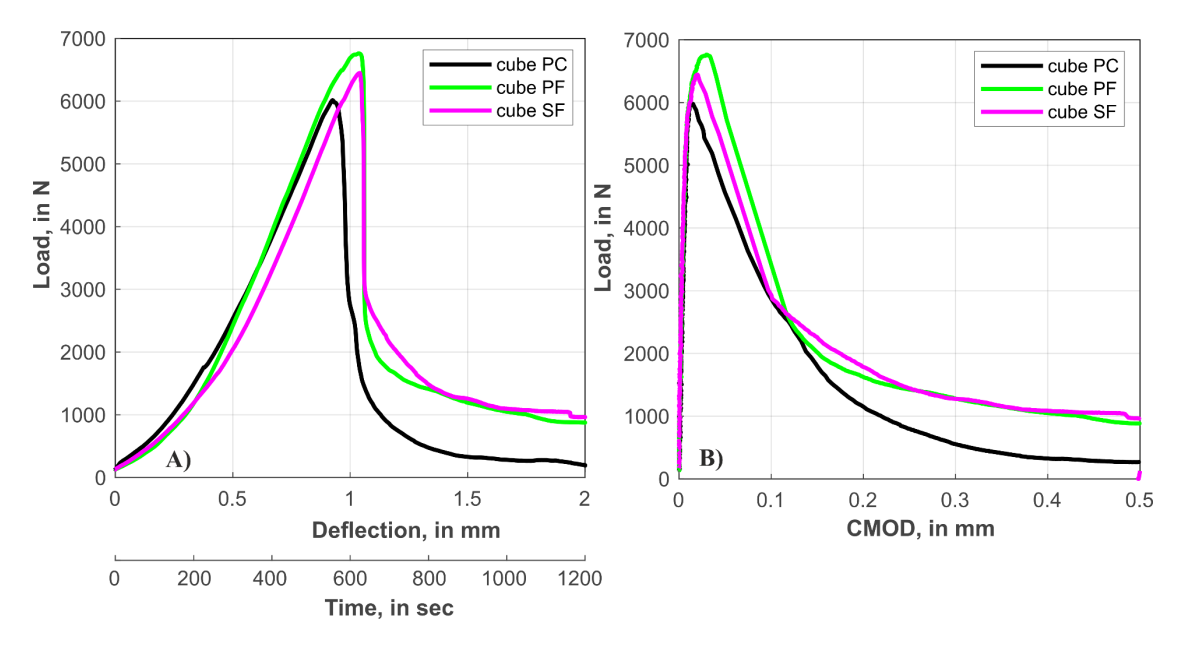


Fig. 3 Splitting test results of tested specimens: A) load-time curves, B) load-CMOD curves.

Acoustic emission results analysis

This section examines the fracture evolution process in all tested samples subjected to the quasi-static splitting test. The assessment was carried out using key AE distribution parameters, including the cumulative number of AE hits and peak amplitude distribution, to monitor and track the progression of damage throughout the testing procedure. AE hit is an important parameter which identifies the extent of microcracking activity and indicates how rapidly the damage grows within the fractured specimens. The higher number of cumulative AE hit rates indicates a greater activity of microcrack initiation and propagation within materials [7]. The amplitudes of AE signals are also used to classify the different failure modes at different time stages within composite specimens [8]. Aslan [8], classified amplitude between (40–50 dB) as matrix cracking, (40–65 dB) as fibre–matrix debonding, (60-80 dB) as fibre pull-out events, and failure breakage amplitudes vary from (80 to 96 dB). The variations in accumulated AE hits and amplitude distribution activity for all tested cubic specimens alongside corresponding load-time curves are depicted in Fig. 4 and Fig. 5, respectively. It can be seen that during the pre-peak stage, all tested specimens exhibited a steady rise in the slope of the cumulative AE hit profile. However, as the specimens reached their peak strength, there was a sudden surge in the gradient of the cumulative AE hit activity, reaching its highest value. This sharp increment signified the transitions of micro-cracks into macro-cracks. In the postcracking phase, the slope of the accumulated AE hit profile steadily decreased before the specimen collapsed, reflecting the progressive degradation in structural integrity.

For the PC specimen, it was observed that a significantly higher number of AE hits was monitored. This indicates that, without reinforcement, internal energy dissipation occurs only through matrix cracking in the PC specimen. Once cracks are initiated, they rapidly propagate, leading to an increased accumulation of microcracks within the matrix. Consequently, the peak loading stage exhibited an increase in high-amplitude AE events. In contrast, the occurrence of high-amplitude AE events during the pre-peak regime was significantly reduced when steel and polyolefin fibres were incorporated into plain concrete. This suggests that microcrack formation was effectively controlled by crack bridging and pull-out event mechanisms provided by the fibres. When cracks initiate, these mechanisms dominate matrix cracking, resulting in energy absorption through the fibre-bridging mechanism and delaying crack propagation. Comparing damage evolution between PF and SF specimens, it was evident that steel fibres were more effective at bridging microcracks than polymer fibres throughout the pre-peak stage. This difference can be explained by the fact that the addition of end-hook-shaped steel fibres results in the creation of a larger fracture surface area and enhances the bridging effect. In contrast, PF fibres (polyolefin), being hydrophobic, exhibited weaker interfacial bonding with the concrete matrix due to poor adhesion. As a result, their ability to bridge microcracks was less effective, leading to fewer AE hits compared to SF. During the post-peak regime, steel fibres generated a higher amplitude AE event than polymer fibres, suggesting a greater ability to resist crack propagation even after peak-load failure. The maximum cumulative number of AE hits recorded were



96125 for SF and 83860 for PF, demonstrating the superior crack bridging ability of steel fibres in maintaining structural integrity beyond the peak load stage.

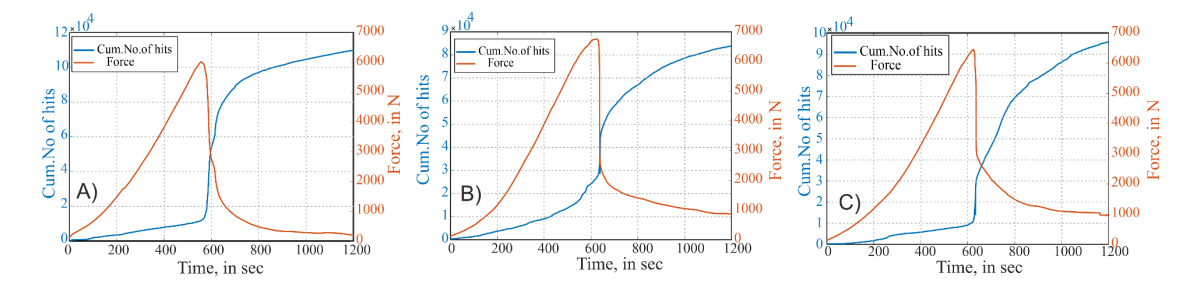


Fig. 4 Typical representation of cumulative AE hits profile for all tested specimens together with loading-time curves: A) cube PC, B) cube PF, C) cube SF.

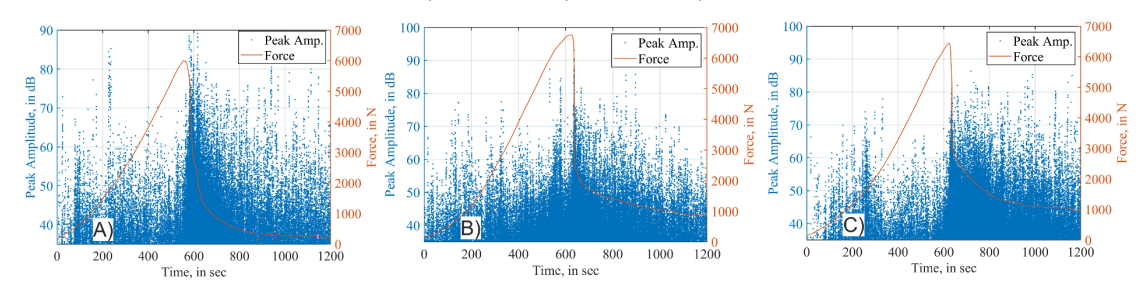


Fig. 5 Amplitude distribution characteristics diagram for all the specimens tested together with loading-time curves: A) cube PC, B) cube PF, C) cube SF.

DIC analysis

The crack locations of all tested cubic specimens were identified using the DIC method, as depicted in Fig. 6. The digital images revealed that the cracking size in the PC sample consistently exceeded the cracking width of the PF and SF samples. Additionally, in the PC specimen, the micro-cracked region expanded rapidly as small cracks merged into larger macro-cracks, indicating a faster progression of the damage. The cracking patterns in PF and SF specimens at 800 were notably similar, with cracks extending across the entire beam length. This suggests that the fibres were completely pulled out from the cracked surfaces, leaving no reinforcement to resist further crack growth, ultimately leading to progressive failure. However, a closer comparison of the DIC images between PF and SF showed that microcracks in SF transitioned into macrocracks more gradually than in PF. This delayed propagation is attributed to the superior crack-arresting ability of steel fibres, which enhance the fibre–matrix interfacial bonding and effectively bridge microcracks, slowing down their expansion compared to PF.

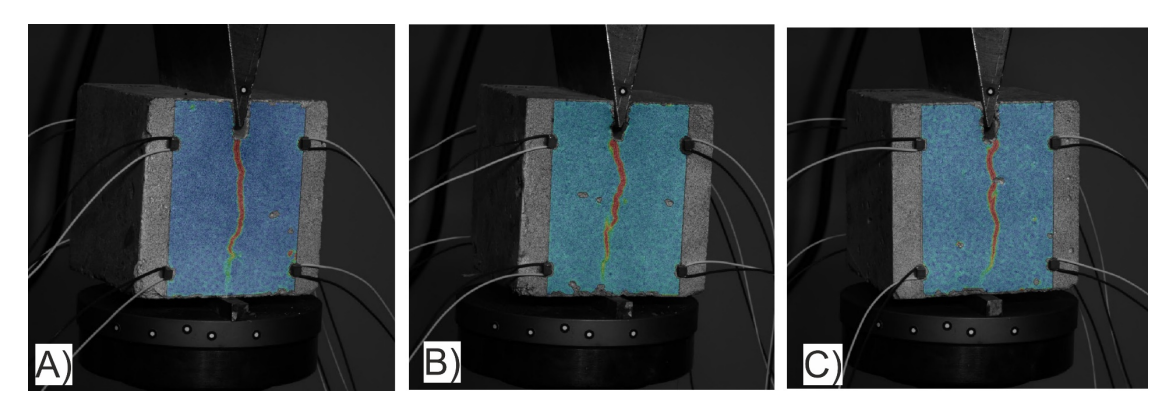


Fig. 6 DIC images for A) cube PC, B) cube PF, C) cube SF specimens at (t = 800 s).



4 DISCUSSION

The experimental results of this work emphasize the real-time monitoring of fracture behaviour in fibre-reinforced concrete cubes with wedge splitting under quasi-static loading. The findings demonstrated that the incorporation of steel and polymer fibres resulted in an increase in the peak load-bearing capacity of fibre-reinforced specimens compared to plain concrete. These fibres have demonstrated the potential to strengthen the bridging mechanism between micro and macro-cracks, thereby increasing the fracture toughness and ductility in fibre-reinforced concrete specimens. Notably, SF exhibited a higher peak-load capacity than PF due to its increased fibre pull-out activities and greater crack-bridging effect, indicating a superior fracture-resistance performance.

The AE analysis results further supported the quasi-static results and provided a damage evolution inside specimens over time. Based on the AE parameter-based AE results it was observed that SF produced higher AE amplitude events during the post-peak regime, reinforcing its superior ability to reduce the crack propagation rate than PF. Furthermore, the DIC analyses highlighted the effectiveness of fibre reinforcement in mitigating crack propagation patterns under the wedge-splitting test. From the DIC images both PF and SF specimens demonstrated a slower crack development as an observed reduction in crack width. However, SF exhibited a slower transition from microcracks to macrocracks than PF, indicating a strong fibre-matrix interfacial bonding between the steel fibres and the concrete matrix, leading to improved load transfer capabilities and exhibiting superior fracture performance and overall structural integrity.

5 CONCLUSION

In this paper, the damage evolution and crack localization in concrete cubic specimens reinforced with PF and SF were analyzed under splitting loads using AE and DIC techniques. The findings obtained based on the experimental results can be drawn as follows.

- The incorporation of steel fibres (SF) and polyolefin fibres (PF) through plain sample markedly enhanced its post-cracking performance in the load-CMOD curves. This improvement can be attributed to the key fibre mechanism, including fibre-matrix debonding, bridging and pull-out events, which effectively contributed to increased resistance against crack propagation and structural integrity retention.
- The parameter-based AE results indicated that fewer high-amplitude AE events were recorded in the SF specimen, demonstrating its superior ability to bridge microcracks than PF. In contrast, PF exhibited weaker interfacial bonding and lower adhesion to the concrete matrix, potentially reducing its effectiveness in microcrack bridging. The maximum cumulative AE hits recorded were 96125 for SF and 83860 for PF specimens.
- DIC image analysis revealed that cracking size in the PC sample consistently exceeded the cracking width
 of the PF and SF samples. However, a comparative analysis of DIC images showed that the microcracks
 in SF transitioned into macrocracks more gradually than in PF, highlighting the enhanced crack-arresting
 capability of steel fibres.
- These findings offer valuable insights for real-time monitoring of microcracks and damage localization in fibre-reinforced structures under WST, ultimately contributing to improved durability and service life.
- This research plays a significant role in advancing SHM applications, thereby enhancing predictive maintenance strategies for fibre-reinforced concrete (FRC) structures.

Acknowledgements

The study was supported by the National Science Centre, Poland, project no. 2019/35/B/ST8/01905.

References

- [1] Carpinteri, A., et al. Influence of damage in the acoustic emission parameters. Cem. Concr. Compos., 44 (2013), pp. 9–16. Available at: https://doi.org/10.1016/j.cemconcomp.2013.08.001
- [2] Thirumalaiselvi, A., and Sasmal, S. Pattern recognition enabled acoustic emission signatures for crack characterization during damage progression in large concrete structures. Appl. Acoust., 175 (2021), 107797.



Available at: https://doi.org/10.1016/j.apacoust.2020.107797

- [3] Hamrat, M., et al. Flexural cracking behavior of normal strength, high strength and high strength fiber concrete beams, using Digital Image Correlation technique. Constr. Build. Mater., 106 (2016), pp. 678–692. Available at: https://doi.org/10.1016/j.conbuildmat.2015.12.166
- [4] Li, D., et al. Experimental study on fracture and fatigue crack propagation processes in concrete based on DIC technology. Eng. Fract. Mech., 235 (2020) 107166. Available at: https://doi.org/10.1016/j.engfracmech.2020.107166
- [5] Sharma, G., et al. Fracture monitoring of steel and GFRP reinforced concrete beams using acoustic emission and digital image correlation techniques. Struct. Concr., 22, no.4(2021), pp.1962-1976. Available at: https://doi.org/10.1002/suco.202000650
- [6] Xu, X., et al. Damage source and its evolution of ultra-high performance concrete monitoring by digital image correlation and acoustic emission technologies. J. Build. Eng., 65 (2023), 105734. Available at: https://doi.org/10.1016/j.jobe.2022.105734
- [7] Geng, J., et al. Studying the dynamic damage failure of concrete based on acoustic emission. Constr. Build. Mater., 149 (2017), pp. 9–16. Available at: https://doi.org/10.1016/j.conbuildmat.2017.05.054
- [8] Aslan, M. Investigation of damage mechanism of flax fibre LPET commingled composites by acoustic emission. Compos. Part B Eng., 54 (2013), pp. 289–297. Available at: https://doi.org/10.1016/j.compositesb.2013.05.042